Electromagnetic and Semiconductor Modeling of Scanning Microwave Microscopy Setups

Author(s):
Gungor, Arif C.; Celuch, Malgorzata; Smajic, Jasmin; Olszewska-Placha, Marzena; Leuthold, Juerg

Publication date:
2020

Permanent link:
https://doi.org/10.3929/ethz-b-000467834

Originally published in:
IEEE Journal on Multiscale and Multiphysics Computational Techniques 5, https://doi.org/10.1109/JMMCT.2020.3027908

Funding acknowledgement:
761036 - Microwave Microscopy for Advanced and Efficient Materials Analysis and Production (EC)

Electromagnetic and Semiconductor Modeling of Scanning Microwave Microscopy Setups

Arif Can Gungor, *Student Member, IEEE*, Malgorzata Celuch, *Member, IEEE*, Jasmin Smajic, *Senior Member, IEEE*, Marzena Olszewska-Placha, *Member, IEEE*, and Juerg Leuthold, *Fellow, IEEE*

***Abstract*—This article presents finite difference time domain (FDTD) and finite element method (FEM) based electromagnetic modeling and simulation of an industrial scanning microwave microscopy (SMM) material measurement setup. These two methods have been employed to cross verify each other for classical electromagnetic simulations of the homogeneous conductive materials under SMM. For the SMM simulations involving semiconductor materials, however, a coupled multiphysics solver is required in addition to the pure electromagnetic analysis. As a solution to this problem, an FEM-based semiconductor Poisson–Drift–Diffusion (PDD) solver and its coupling to transient electromagnetic solver is presented in this article. The considered SMM setup consists of a conductive fine tip suspended at a certain height above the sample. For the validation purposes of electromagnetic solvers, the numerical modeling was based on both the time domain FEM (TD-FEM) and FDTD. Both numerical methods extract the scattering parameters from the computed field of the conductive or dielectric samples. At the second stage of the analysis, the TD-FEM solver is coupled with the time domain PDD semiconductor solver in order to simulate charge transport and explain behavior of the charges in semiconducting domains under electromagnetic illumination similar to SMM setups.**

***Index Terms*—Electromagnetic modeling, finite difference time domain (FDTD), finite element method (FEM), frequency and time domain methods, materials modeling, multiphysics simulations, scanning microwave microscopy (SMM).**

I. Introduction

DEVELOPMENTS of new organic and inorganic materials are currently at the focus of industrial needs. The quality and performance of the final manufactured products depend strongly on their chemical/electrical/optical/mechanical properties at nanoscale as well as their arrangements at macroscale. While nanoscale measurements have become feasible [1]–[5], macroscale characterization as in [5]–[7] is needed to verify that the material properties are set correctly on the entire surface of, e.g., a thin-film solar cell. To bridge the gap between nano- and macroscale measurements, and to interpret those measurements into industrially useful knowledge, numerical modeling techniques are needed that replicate the measurement process on a computer and visualize the otherwise invisible physical phenomena.

This work forms a part of our research activities conducted in the framework of the European project MMAMA [8] concerned with scanning microwave microscopy (SMM), its modeling, and simulation. SMM is a family of material measurement techniques at microwave frequencies, from micro- to nanoscale. A representative setup for nanoscale is SMM tips [1]–[5], while popular macroscale setups also include dielectric resonators [5]–[7] very frequently. The modeling of those setups has previously been reported [1]–[7]. However, for the sharp tip-to-sample interaction, the focus has typically been on a specific problem, for which an overall understanding was required [5], and the models were only based on electromagnetic solvers limiting samples to homogeneous dielectrics and metals excluding semiconductors, which requires a multiphysics solver. In this article, we summarize our efforts to apply the widely used finite element methods (FEM) (in the form of in-house developed field solvers) [8], [9] and finite difference time domain (FDTD) methods [10], [11] (in the form of customized regimes for operating commercial solvers) to the analysis of SMM scenarios, with a view to setting up a computer platform flexible in terms of geometry and simulation parameters. In addition, we report detailed quantitative results for SMM of homogeneous dielectric and metallic samples using the mentioned electromagnetic solvers. Furthermore, a complete study of modeling of semiconductors is presented, an FEM-based solver to handle semiconductor equations in 2-D, and a coupling algorithm with the time domain electromagnetic solver is developed. FEM is chosen to develop the coupled solver thanks to its capabilities of efficient multiphysics coupling and irregular structure coverage over FDTD, and this coupled solver enables to simulate SMM of semiconductors with high accuracy. Even though there has been coupled transient solvers that address modeling the multiphysics for certain semiconductor devices (such as lasers [12]) a general purpose transient solver that is capable of multiphysics modeling of any semiconductor structure has not been reported before, to the best knowledge of the authors.

This article is organized as follows. Section II presents electromagnetic analysis of a tip-to-sample interaction by using FEM and FDTD, which has also led to cross-validation of the said numerical approaches with a high agreement level. Section III

Manuscript received March 28, 2020; revised June 5, 2020 and July 24, 2020; accepted September 2, 2020. Date of publication September 30, 2020; date of current version October 26, 2020. This work was supported by the European Union's Horizon 2020 research and innovation programme (H2020-NMBP-07-2017) under Grant agreement MMAMA 761036. *(Corresponding author: Arif Can Gungor.)*

Arif Can Gungor, Jasmin Smajic, and Juerg Leuthold are with the Institue of Electromagnetic Fields, ETH Zürich, 8092 Zürich, Switzerland (e-mail: arifg@ethz.ch; jasmin.smajic@ief.ee.ethz.ch; leuthold@ethz.ch).

Malgorzata Celuch and Marzena Olszewska-Placha are with the QWED, 02-078 Warsaw, Poland (e-mail: mceluch@qwed.eu; molszewska@qwed.eu).

Digital Object Identifier 10.1109/JMMCT.2020.3027908

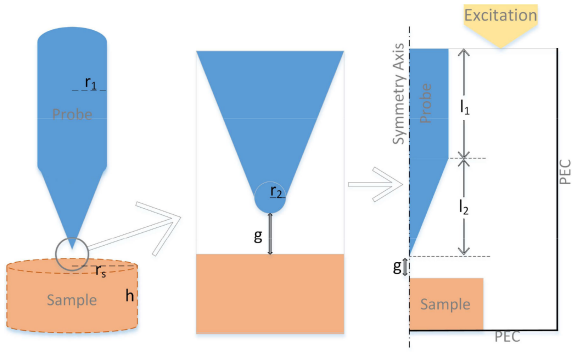

Fig. 1. Visualization of the considered conductive SMM tip in 3-D (left), fine tip and the gap (middle) and in 2-D using axial symmetry (right).

describes the FEM-based transient semiconductor solver along with an algorithm to handle nonlinear, coupled semiconductor equations. Section IV describes the coupling algorithm of the developed solvers and summarizes the results. Section V discusses the results and indicates other possible scenarios and further steps required for a more advanced semiconductor solver and concludes this article.

II. Transient Electromagnetic Analysis of SMM Tip

The tip-to-sample SMM problem considered for this analysis is based on an industrial definition [13] and visualized in Fig. 1. It has a straight conductive section with length $l_1 = 1.5$ mm and radius $r_1 = 0.5$ mm, which is tapered into a sharp tip with length $l_2 = 1.5$ mm and minimum radius of $r_2 = 25$nm. The tip is suspended above the sample at a certain distance of $g = 100$ nm to account for near field microscopy and also rounded with radius r_2 to avoid causing singularities during the numerical analysis. Four samples with different properties are considered: perfect electric conductor (PEC), metal (representing gold with $\varepsilon_r = 1$, $\sigma = 4 \cdot 10^7$ S/m), lossless dielectric (representing silicon nitride of $\varepsilon_r = 10$), and lossy dielectric (representing bulk silicon of $\varepsilon_r = 10, \sigma = 100$ S/m). The scattering response around 10 GHz band is of our interest.

A general-purpose axisymmetric FDTD code [14] is first applied with TEM pulse excitation over 8–12 GHz band launched from the port on top of Fig. 3 (right). The excitation corresponds to the fundamental TEM mode of a coaxial line. The spatial discretization near the fine tip and the air gap can be seen in Fig. 2 for both the solvers. Very high aspect ratio makes the overall geometry quite challenging due to its whole domain size in millimeter scale and the tip radius in nanometer scale. It is observed that for some combinations of the geometry and material data, FDTD analysis with a standard GPU code has issues with converging and the reflection coefficient results are corrupted with a numerical noise, after thousands of excitation periods. This is attributed to the very fine meshing at the SMM tip that is needed to model the tip and the gap (FDTD cells as small as 25 nm near the tip creating up to 50 000 cells in total). Therefore, a double-precision version of the FDTD code is implemented. The GPU version is always used as the first tool

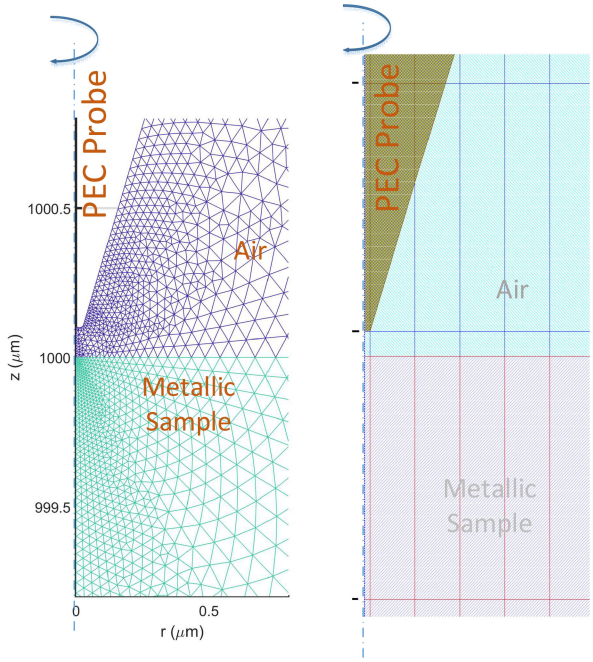

Fig. 2. Very fine discretization near the fine tip ($r_2 = 25$ nm) for TD-FEM (left) and FDTD (right) solvers.

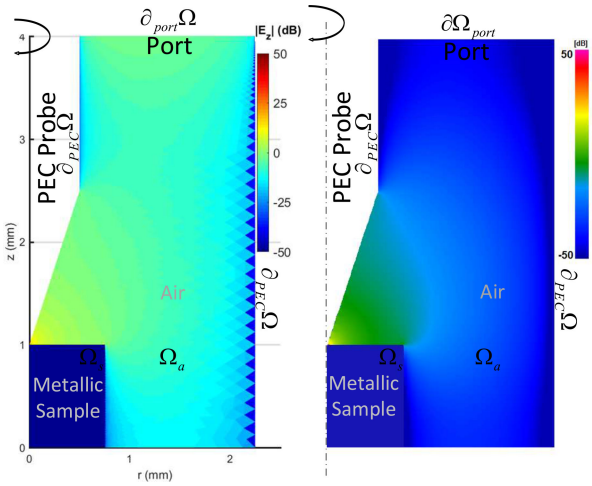

Fig. 3. Amplitude of z-component of E-field profile obtained using TD-FEM (left) and FDTD (right), showing similar behavior with the same port excitation and metallic sample.

and the double-precision version is resorted for the cases with convergence issues.

With the said improvements, the FDTD simulations converge after 5 min of the GPU time, and the required memory is within 4 MB. The metals are modeled with the surface impedance model that is applied along the metal surface to represent frequency dependent skin effect as in [15].

For visualization purposes, the z-component of the electric field profile is depicted in Fig. 3 at a chosen time step with metallic sample, and the effects of different samples are distinguished in scattering parameters, as shown in Fig. 4.

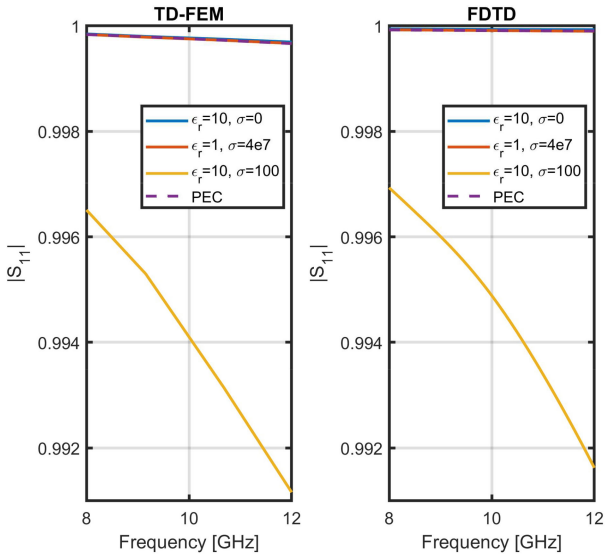

Fig. 4. Reflection from metallic and dielectric samples with the tip-to-sample gap of 100 nm obtained with FDTD (right) and TD-FEM (left), without port calibration.

To conduct transient FEM simulation, we implemented a time-domain algorithm (TD-FEM) with vector edge elements and linear shape functions to solve time domain E-field wave equation. Moreover, the selection of time domain implementation of the electromagnetic solver also enabled us to couple it to the transient semiconductor physics solver extending the capabilities of the SMM model considerably, as demonstrated in Sections III and IV. Then, extracting the port scattering parameters and analyzing the Fourier transform of the applied signal would show the effects of different sample properties on the reflected power.

The following E-field wave equation describes the electromagnetic wave propagation within the simulation model:

$$\nabla \times \frac{1}{\mu}\nabla \times \mathbf{E} + \mu_0\sigma\frac{\partial \mathbf{E}}{\partial t} + \mu_0\varepsilon_0\varepsilon_r\frac{\partial^2 \mathbf{E}}{\partial t^2} = 0 \ \text{ in } \Omega_a \cup \Omega_s = \Omega \subset R^2. \tag{1}$$

The boundary condition on the excitation port has the following form:

$$\mathbf{a_n} \times \left(\frac{1}{\mu}\nabla \times \mathbf{E}\right) + \frac{\mu_0}{Z_{\text{Port}}}\mathbf{a_n} \times \left(\mathbf{a_n} \times \frac{\partial \mathbf{E}}{\partial t}\right) = \frac{-2\mu_0}{Z_{\text{Port}}}\,\mathbf{a_n} \times \left(\mathbf{a_n} \times \frac{\partial \mathbf{E}_0}{\partial t}\right) \ \text{over} \ \partial_{\text{port}}\Omega \subset R^1 \tag{2}$$

where $\mathbf{a_n}$ denotes the unit normal vector to the respective boundary, Z_{Port} is the wave impedance at the port, and $\mathbf{E}_0$ is the input excitation field from the port, which represents the fundamental TEM mode of the coaxial structure and in time domain has a shape of a well-known Gaussian burst with center frequency of 10 GHz [8].

The bottom and right boundaries of the domain in Fig. 3 are taken as PEC ($\mathbf{a_n} \times \mathbf{E} = 0$ over $\partial_{\text{PEC}}\Omega$) and the left boundary conditions at $r = 0$ represents the axial symmetry of the problem ($\mathbf{a_n} \times \frac{1}{\mu}\nabla \times \mathbf{E} = 0$). The weak form of the equation is obtained by applying the Galerkin's variant of the weighted residual method [9] where $\mathbf{E^c}$ denotes the trial vector function for the unknown vector field $\mathbf{E}$. For the time-discretization, the following backward difference formula (BDF) is used:

$$\frac{\partial \mathbf{E}}{\partial t} \approx \frac{\mathbf{E_t} - \mathbf{E_{t-1}}}{\Delta t} \tag{4}$$

where subscripts denote the time steps and (3), shown at the bottom of the page, is solved for $\mathbf{E_t}$ after substituting (4).

For the structure defined in Fig. 1, the implemented FEM solver utilizes a mesh with around 85 000 elements with very fine elements (a few nanometer edge size) near the sharp tip, 127 000 edges (degree of freedom) requiring less than 200 MB of RAM, excluding the memory needed to store all field values for visualization. A standalone solver in the form of a C++ code was developed and compiled. For the simulated example case, around 1000 time steps with $\Delta t = 2$ ps were needed for the analysis to converge, taking less than 10 min of the CPU time. Choosing such small time steps is also important in order to minimize the possible energy loss due to BDF time stepping. Hence, in this case, the time domain FEM is computationally more expensive than FDTD, both in terms of the memory and simulation time. This is especially because the employed algorithm is implicit and computationally costly matrix operations are performed thousands of time for finding the transient solution. However, the time domain FEM approach makes the coupling with transient nonlinear semiconductor solver possible, which is described in the following sections.

After solving the time domain E-field wave equation, the electric field distribution at a chosen time step can be visualized as shown in Fig. 3, and the port parameters are extracted to obtain the scattering parameters, as depicted in Fig. 4. The scattering parameters calculated with TD-FEM and FDTD are in good agreement, which cross-validates the presented field solvers. As expected, lossy dielectric sample causes lower reflections than the lossless cases, and the reflections decrease with frequency. The obtained field distribution profiles at the same time instant from both solvers are quite similar and predict the same levels of electromagnetic field intensities in the z-direction near the tip-sample junction as presented in Fig. 3.

$$\iint_{\Omega}\left\{ r\left(\frac{1}{\mu}\nabla \times \mathbf{E}\right)\cdot(\nabla \times \mathbf{E^c}) + \mu_0\sigma r\mathbf{E^c}\cdot\frac{\partial \mathbf{E}}{\partial t} + \mu_0\varepsilon_0\varepsilon_r\mathbf{E^c}\cdot\frac{\partial^2 \mathbf{E}}{\partial t^2}\right\} dS + \frac{\mu_0}{Z_{\text{Port}}}\int_{\partial_{\text{port}}\Omega} r\,(\mathbf{a_n} \times \mathbf{E^c})\cdot\left(\mathbf{a_n} \times \frac{\partial \mathbf{E}}{\partial t}\right) dl = \frac{-2\mu_0}{Z_{\text{Port}}}\int_{\partial_{\text{port}}\Omega} r\,(\mathbf{a_n} \times \mathbf{E^c})\cdot\left(\mathbf{a_n} \times \frac{\partial \mathbf{E}_0}{\partial t}\right) dl \tag{3}$$

III. Transient Analysis of Semiconductor Physics

The previously elaborated tip-to-sample SMM model is capable of modeling materials with constant conductivity. However, SMM of materials and devices that are based on semiconductors reacts to external electromagnetic field and the local conductivity within semiconductor domain changes accordingly due to charge movement. In other words, the external field creates depleted or accumulated regions in the semiconductor near the sharp tip, which then changes the reflections due to the position dependent electric conductivity. Modeling of this change requires multiphysics simulations, where the transient semiconductor physics is also analyzed along with full Maxwell's equation system. Thus, the behavior of charges within semiconductor domains is accurately modeled and their microwave scan can be better understood and explained. The previously presented transient TD-FEM full Maxwell solver was developed with the aim to facilitate multiphysics coupling with presented semiconductor solver. This section presents in detail the simulation algorithm adopted from [16] and [19] used for semiconductor regions in axisymmetric structures and its coupling to the electromagnetic solver using FEM.

The basic set of equations governing transient semiconductor behavior based on the well-known Poisson-drift-diffusion theory can be written in the following form [16]:

$$\nabla^2\varphi - \mu\varepsilon\frac{\partial^2}{\partial t^2}\varphi = -\frac{q}{\varepsilon}\left(p - n + N_d^+ - N_a^-\right) \tag{5}$$

$$\nabla\cdot\mathbf{J_p} = -q\left(R + \frac{\partial p}{\partial t}\right) \tag{6}$$

$$\nabla\cdot\mathbf{J_n} = q\left(R + \frac{\partial n}{\partial t}\right) \tag{7}$$

$$\mathbf{J_p} = qp\mu_p\left(-\nabla\varphi\right) - qD_p\nabla p \tag{8}$$

$$\mathbf{J_n} = qn\mu_n\left(-\nabla\varphi\right) + qD_n\nabla n \tag{9}$$

where φ is the electric potential, $n(p)$ is the electron (hole) concentration, R is the net generation-recombination rate of carriers, $\mathbf{J_n}$ ($\mathbf{J_p}$) is the electron (hole) current density, N_d^+ and N_a^- are the ionized donor and acceptor charge densities due to doping, μ_n (μ_n) is the electron (hole) mobility, $D_n(D_p)$ is the electron (hole) diffusion coefficient, ε and μ are the electric permittivity and magnetic permeability of semiconductor material, respectively, and q ($= 1.602\cdot10^{-19}C$) is the elementary charge.

Equation (5) is the wave equation for electric potential, (6) and (7) are the continuity equations for the charge carriers. This set of equations is supplemented by carrier transport equations (8) and (9), which take both drift and diffusion of charges into account. For the next generation-recombination rate of the charges, the widely used Read–Hall–Shockley recombination mechanism ($R = \frac{np}{\tau_n(p+n_i)+\tau_p(n+n_i)}$, where average life times for the carriers are taken as $\tau_n = \tau_p = 10\ \mu$s, and $n_i = 9\cdot10^9\text{cm}^{-3}$ is the intrinsic carrier concentration) is assumed [16].

The parameters of the model are scaled by using the normalization factors [17] given in Table I, in order to avoid scaling issues (ill conditioning) that might arise in numerical analysis.

TABLE I
Normalization Factors Used for Scaling of Equations

Quantity ($V_{real} = V_{norm}Factor$)	Normalization factor	
	Symbol	Value
Time (t)	L_0/D_0	$1.583\cdot10^{-6}$ (s)
Position ($\mathbf{r}$)	$L_0 = \sqrt{\varepsilon V_t/qn_i}$	$4{,}339\cdot10^{-3}$ (cm)
Electric scalar potential (ϕ)	$V_t = k_BT/q$	$2.586\cdot10^{-2}$ (V)
Electric field ($\mathbf{E} = -\nabla\phi$)	V_t/L_0	5.96 (V/cm)
Electron density (n)	n_i	$8{,}954\cdot10^9$ (cm^{-3})
Hole density (p)	n_i	$8{,}954\cdot10^9$ (cm^{-3})
Generation-Recombination (G)	D_0n_i/L_0^2	$5.657\cdot10^{15}$ (cm^{-3}/s)
Diffusion constants ($\gamma_n^{-1}, \gamma_p^{-1}$)	D_0	11,896 (cm^2/s)
Mobilities ($\gamma_n^{-1}, \gamma_p^{-1}$)	D_0/V_t	460 (cm^2/Vs)
Current densities ($\mathbf{J_n}, \mathbf{J_p}$)	D_0qn_i/L_0	$3{,}932\cdot10^{-6}$ (A/cm^2)

A variant of Gummel's method [18] is proposed for decoupling and discretization of set of equations where the Poisson equation and carrier conservation equations are solved iteratively until a convergence is reached. The matrix formulation of the weak forms of the system is obtained by using the Galerkin's method of weighted residuals [8], [19]

$$\left[F^{(1)}\right]\ \{\phi\} = \left[F^{(2)}\right]\ (\{p\} - \{n\} + \{N_A\} - \{N_D\}) \tag{10}$$

$$\left[F^{(2)}\right]\frac{\partial}{\partial t}\ \{n\} = \gamma_n^{-1}\ [D]\{n\} - \gamma_n^{-1}\left[F^{(1)}\right]\{n\} + \left[F^{(2)}\right]\{G\} \tag{11}$$

$$\left[F^{(2)}\right]\frac{\partial}{\partial t}\ \{p\} = -\gamma_p^{-1}\ [D]\{p\} - \gamma_p^{-1}\left[F^{(1)}\right]\{p\} + \left[F^{(2)}\right]\{G\}. \tag{12}$$

Here, the matrices are defined based on finite element formulation with linear shape functions (N_i) as in (13)–(15) [8], [19]. The vector $\{G\}$ stands for net generation rate and is taken as $G = -R$ throughout this article. Moreover, (5) is reduced to Poisson equation with discretized form seen in (10) since the dimensions of the simulation domain is much smaller than the shortest wavelength of the excitation considered

$$F^{(1)}{}_{ij} = \sum\iint_\Omega \nabla N_i\cdot\nabla N_j d\Omega \tag{13}$$

$$F^{(2)}{}_{ij} = \sum\iint_\Omega N_iN_j d\Omega \tag{14}$$

$$D = \sum\nabla\phi^e\cdot\iint_\Omega \nabla N_i\ N_j d\Omega. \tag{15}$$

BDF (4) for time discretization is again employed, and the set of matrix equations consequently takes the following form:

$$[F^{(1)}]\{\phi\}^{\text{t+1}} = [F^{(2)}](\{p\}^{t+1} - \{n\}^{\text{t+1}} + \{N_A\} - \{N_D\}) \tag{16}$$

$$([F^{(2)}] - \Delta t\gamma_n^{-1}[D] + \Delta t\gamma_n^{-1}[F^{(1)}])\ \{n\}^{\text{t+1}} = [F^{(2)}]\ \{n\}^t + [F^{(2)}]\{G\}^t \tag{17}$$

$$([F^{(2)}] - \Delta t\gamma_p^{-1}[D] + \Delta t\gamma_p^{-1}[F^{(1)}])\ \{p\}^{t+1} = [F^{(2)}]\ \{p\}^{t} + [F^{(2)}]\{G\}^{t}. \quad (18)$$

Here, subscript t denotes the time steps whereas subscript i is used to denote the under relaxation iterations as in (19) and (20). The decoupled set is then solved for each time step t in an iterative manner as follows: first, the Poisson equation (16) is solved to obtain potential distribution within the domain, which is then included in $[D]$ to update the carrier distribution accordingly using (17) and (18). The emerging solutions of (17) and (18) are named as $\{n\}_{\text{new}}^{t+1}$ and $\{p\}_{\text{new}}^{t+1}$. Due to nonlinear nature of the latter two equations, instead of directly assigning $\{n\}^{t+1}$ and $\{p\}^{t+1}$ from solution of (17) and (18), an under relaxation method is utilized as in (19) and (20). Then, the updated carrier concentrations are inserted back into (16) establishing a closed loop simulation which runs until convergence as defined in (21) with respect to all the three unknowns is reached for the time step t. Then, the solver assigns the latest iterations of the unknown vectors to the $(t+1)$th time step and moves to the computation of the next time step. Here, the methods described in [19] for 1-D semiconductors are adopted to account for considered 2-D Cartesian and axisymmetrical structures. The dynamic relaxation parameter α is initially set to a small number (0.01 proves to be a good starting point) and adaptively changes between 0 and 1, as the system is getting closer to a converged state

$$\{n\}_{\text{i+1}}^{t+1} = (1-\alpha)\ \{n\}_{\text{i}}^{t+1} + \alpha\,\{n\}_{\text{new}}^{t+1} \quad (19)$$

$$\{p\}_{\text{i+1}}^{t+1} = (1-\alpha)\ \{p\}_{\text{i}}^{t+1} + \alpha\,\{p\}_{\text{new}}^{t+1}. \quad (20)$$

By controlling contribution of the new set of solutions, iterative under relaxation method avoids nonphysical spurious oscillatory behavior caused by nonlinearities, which might result negative carrier concentrations and divergence of equations. Furthermore, at every iteration the residual for the variables are checked and the simulation continued until the norm of the residual as defined for electron concentration in (21) for all unknowns is less than 10^{-6}

$$\rho_n = \left| \frac{\{n\}_{\text{new}}^{t+1} - \{n\}_{\text{i+1}}^{t+1}}{\{n\}_{\text{i+1}}^{t+1}} \right| < 10^{-6}. \quad (21)$$

This suggested method is verified by simulating 1-D and 2-D pn-junction diodes with varying bias. The simulation results for charge behavior, device currents, and formation of depletion region show a great agreement with the analytical calculations, as shown in Fig. 5.

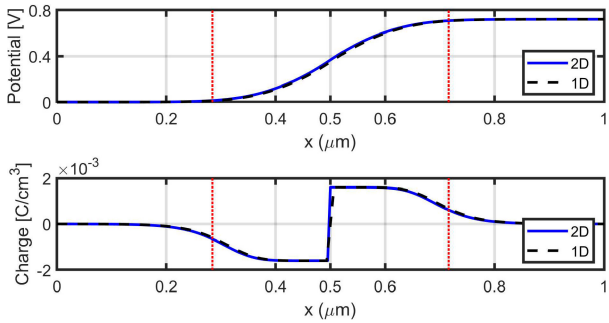

Fig. 5. Simulation results show the built-in potential (top) and the total charge distributions (bottom) for a pn junction with zero bias. The simulated diode has p-type doping ($N_A = 10^{16}$ cm^{-3}) on the left half ($x < 0.5$ μm) and n-type doping ($N_D = 10^{16}$ cm^{-3}) on the right half (0.5 μm $< x <$ 1 μm), and its height is 0.1 μm for 2-D case. The 1-D PDD solver is run for 1-D pn junction diode with the same doping profile. The data shown for 2-D simulation is extracted from the mid-line (at $y = 0.05$ μm). Red lines show the extents of the depletion region based on analytical calculations [16].

Algorithm

Input: The *initial guess* for ϕ, p, and n in semiconductor domains
run *Stationary semiconductor solver* to obtain initial conditions for ϕ, p, and n in semiconductor domains
for time steps t=1, 2,.., N_t **do**
  while not converged **do**
    run *Transient EM solver* using the spatial conductivity *σ obtained from charge distribution to solve for field distribution*
    run *Transient semiconductor (SC) solver using the drift-diffusion currents and the current caused by external field to obtain the charge distribution*
    check residuals for convergence
  end while
end for

Fig. 6. Coupling algorithm between the transient full Maxwell solver and the semiconductor Poisson-drift-diffusion solver.

IV. TD-FEM Coupled Electromagnetic and Semiconductor Solvers

Developing a stable semiconductor solver in time domain also enables us to develop an algorithm to couple the solver with previously described transient electromagnetic solver for simulation of SMM involving semiconductor materials.

The coupling between the solvers is established by using an iterative approach as presented in Fig. 6. As the first step, before the time marching is started, the initial conditions for the charge and potential distributions in semiconductor domains are obtained by using the stationary values from the semiconductor solver. Afterward, the spatial conductivity σ (for semiconductor domains $\sigma = qp\mu_p + qn\mu_n$), that is used in transient full Maxwell solver, is updated using the obtained charge distributions p and n. Next, the time stepping starts and the electromagnetic field distribution is obtained in all the domains using the transient electromagnetics solver. Then, the transient semiconductor solver delivers the charge carrier densities in the corresponding domains by taking into account the currents caused by the external excitation field $\mathbf{E_t}$. The total electric field at any step can be considered as the sum of the divergence free external field $\mathbf{E_t}$and the curl-free part due to charges in the semiconductor: $\mathbf{E}_t^{\text{total}} = \mathbf{E_t} - \nabla\varphi$ (i.e., for the electrons the total electron current that is taken into account with the semiconductor solver

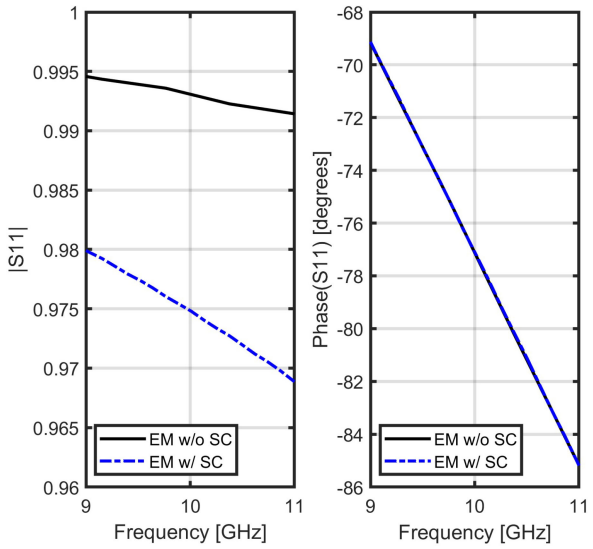

Fig. 7. Scattering parameters (S_{11}) obtained from an n-doped (with doping of 10^{16} cm^{-3}) semiconductor sample with and without the coupled semiconductor (SC) physics solver.

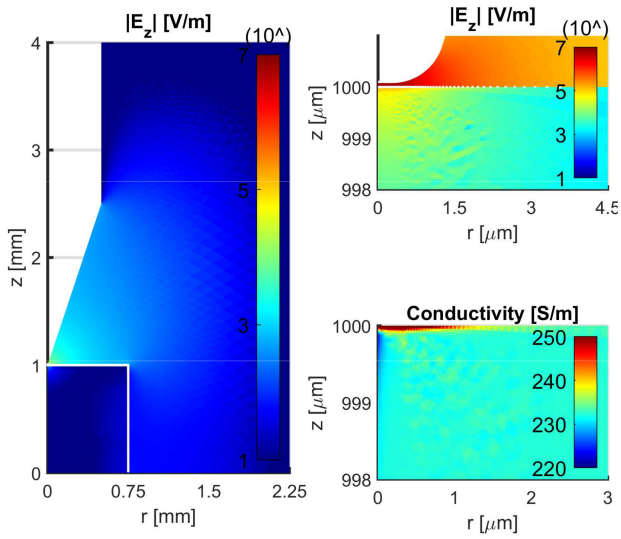

Fig. 8. Amplitude of z-component of E-field profile everywhere (left), near the rounded fine tip (top right), and the variation of conductivity in the semiconductor near the tip (bottom right) at a chosen time step, obtained from multiphysics simulation of SMM of an n-doped semiconductor sample (with doping of 10^{16} cm^{-3}) ($r = 0$ is the symmetry axis and the limits of the semiconductor sample domain depicted with white dots).

can be updated as $\boldsymbol{J_n} = qn\mu_n \boldsymbol{E_t} + qn\mu_n(-\nabla\varphi) + qD_n\nabla n$. The newly obtained charge distribution is provided back into the electromagnetic solver in order to initiate the next iteration. The described strongly coupled, i.e., both physics share the same time step, iterative multiphysics simulation loop continues for each time step until all the unknowns converge (i.e., until they reach stable spatial distributions with respective residuals below 10^{-6}), before moving onto the next time step. The coupled simulation performed with a few thousand time steps in order to cover a Gaussian Burst signal that is centered at 10 GHz. The experiments have revealed that for sufficiently small time steps (in the order of a few picoseconds) with dynamically changing relaxation parameter α, the coupled solver converges nicely for each time step also conserving the energy and the charge.

The scattering parameters simulated for the setup in Fig. 1 are obtained for an n-doped ($N_D = 10^{16}$cm^{-3}) semiconductor sample and they are presented in Fig. 7, and the difference in reflected power calculation with or without the semiconductor solver is evident, clearly showing the need to simulate semiconductor physics for accurately capturing important SMM phenomena. This difference is caused by the moving charges as they accumulate (or deplete depending on the sign of the field and doping type) from the surface of the semiconductor region as the external field changes as shown in Fig. 8.

Due to the air gap between the tip and the sample, most of the electric field reflects from the tip-air junction; in other words, the coupling of the field into the sample is reduced considerably due to the air gap. The modeled tip for this simulation has radius of $r_2 = 1$ μm, which also reduces the effects caused by the sample. It is likely to observe a greater difference with a touching or even a wider tip. However, for the consistency of this article, the coupled algorithm is demonstrated for the setup with an air gap (50 nm) similar to the one in Fig. 1, with slightly wider tip.

V. Conclusion

In this article, FDTD and FEM methods have been applied to a scenario representative of industrial SMM material measurement setup: a tip-to-sample interface. Since the scenarios are axially symmetrical, computationally effective 2-D bodies-of-revolution variants of both methods are applicable. In addition, a multiphysics solver capable of solving semiconductor physics coupled with electromagnetics is also presented and applied to the tip-to-sample SMM setup for higher accuracy modeling of semiconductor samples.

For axisymmetric FDTD, the commercial tool available in [14] has been used as a starting point but adapted to the high accuracy requirements of the SMM. For FEM, in-house solvers have been developed for electromagnetics simulations. The proposed FEM solver is a time-domain edge element based solver used with locally refined meshes to accurately model the electromagnetic coupling of the fine tip with the sample. For the transient problem, FEM and FDTD are able to simulate the structure and detect the minimal effects of the material samples on the reflection coefficient of the considered scenario. They are consistent with the measurements [13] in indicating the higher reflections caused by the dielectric as compared to the metal, and the decrease of reflections with frequency. As expected, FDTD is more effective than TD-FEM for the transient electromagnetics problem. However, TD-FEM offers more flexibility for easier multiphysics coupling. In the second part of the work, a transient Poisson-Drift-Diffusion-based semiconductor solver has been developed using TD-FEM. And the developed TD-FEM semiconductor solver is coupled with electromagnetic solver in order to compute carrier transport in semiconductors materials during SMM. This leads to full-complexity SMM simulations with accurate modeling of semiconductor samples.

The results demonstrate a difference in scattering parameters when the semiconductor solver is employed, which proves the importance of coupled multiphysics solver for highly accurate SMM simulations required by semiconductor industries.

The proposed multiphysics simulation algorithm can also be used for simulations of SMM for advanced samples with layers of different types of materials or device structures with regions of different doping. Additionally, the flexible nature of FEM enables to introduce other physical phenomena such as light absorption or other carrier generation-recombination mechanisms, which might be relevant for other semiconductor structures and applications.

REFERENCES

[1] J. H. Lee, S. Hyun, and K. Char, "Quantitative analysis of scanning microwave microscopy on dielectric thin film by finite element calculation," *Rev. Sci. Instrum.*, vol. 72, no. 2, pp. 1425–1434, Jan. 2001.

[2] K. Lai, W. Kundhikanjana, M. Kelly, and Z. X. Shen, "Modeling and characterization of a cantilever-based near-field scanning microwave impedance microscope," *Rev. Sci. Instrum.*, vol. 79, no. 6, Jun. 2008, Art. no. 063703.

[3] T. Wei, X. D. Xiang, W. G. Wallace-Freedman, and P. G. Schultz, "Scanning tip microwave near-field microscope," *Appl. Phys. Lett.*, vol. 68, no. 24, pp. 3506–3508, Apr. 1996.

[4] J. Hoffmann, G. Gramse, J. Niegemann, M. Zeier, and F. Kienberger, "Measuring low loss dielectric substrates with scanning probe microscopes," *Appl. Phys. Lett.*, vol. 105, no. 1, pp. 013102-1–013102-4, Jul. 2014.

[5] A.C. Gungor, M. Celuch, J. Smajic, M. Olszewska-Placha, and J. Leuthold, "Flexible electromagnetic modeling of SMM setups with FE and FDTD methods," in *Proc. IEEE MTT-S Int. Conf. Numer. Electromagn. Multiphys. Model. Optim.*, May 29–31, 2019, pp. 1–4.

[6] J. Krupka and J. Mazierska, "Contactless measurements of resistivity of semiconductor wafers employing single-post and split-post dielectric-resonator techniques," *IEEE Trans. Instrum. Meas.*, vol. 56, no. 5, pp. 1839–1844, Oct. 2007.

[7] J. Krupka, K. Derzakowski, A. Abramowicz, M. E. Tobar, and R. G. Geyer, "Use of whispering-gallery modes for complex permittivity determinations of ultra-low-loss dielectric materials," *IEEE Trans. Microw. Theory Tech.*, vol. 47, no. 6, pp. 752–759, Jun. 1999.

[8] J.-M. Jin, *The Finite Element Method in Electromagnetics*, 3rd ed. New York, NY, USA: Wiley, 2014.

[9] J. Smajic, *How to Perform Electromagnetic Finite Element Analysis*. Hamilton, U.K.: NAFEMS, Ltd., 2016.

[10] A. Taflove and S. C. Hagness, *Computational Electrodynamics—The Finite-Difference Time-Domain Method*, 3rd ed. Boston, MA, USA: Artech House, 2005.

[11] M. Celuch and W. K. Gwarek, "Industrial design of axisymmetrical devices using a customized FDTD solver from RF to optical frequency bands," *IEEE Microw. Mag.*, vol. 9, no. 6, pp. 150–159, Dec. 2008.

[12] C. Fischer and R. Schuhmann, "Transient simulation of cylindrical laser cavities containing active media," in *Proc. Int. Conf. Electromagn. Adv. Appl.*, 2012, pp. 518–521.

[13] H2020 MMAMA project reports, 2020. [Online]. Available: https://www.mmama.eu

[14] QuickWave EM Software, 2020. [Online]. Available: https://www.qwed.eu

[15] M. Celuch-Marcysiak, W. Gwarek, and M. Sypniewski, "A simple and effective approach to FD-TD modelling of structures including lossy metals," in *Proc. Asia-Pacific Microw. Conf. Proc.*, Dec. 1998, pp. 991–993.

[16] S. M. Sze and K. K. Ng, *Physics of Semiconductor Devices*. Hoboken, NJ, USA: Wiley, 2006.

[17] D. M. Andrea, "Accurate numerical steady-state and transient one-dimensional solutions of semiconductor devices," Ph.D. dissertation, California Inst. Technol., Pasadena, CA, USA, 1968.

[18] H. K. Gummel, "A self-consistent iterative scheme for one-dimensional steady state transistor calculations," *IEEE Trans. Electron. Devices*, vol. ED-11, no. 10, pp. 455–465, Oct. 1964.

[19] A. C. Gungor, J. Smajic, F. Moro, and J. Leuthold, "Time-domain coupled full Maxwell- and drift-diffusion-solver for simulating scanning microwave microscopy of semiconductors," in *Proc. Prog. Electromagn. Res. Symp.*, Jun. 2019, pp. 4071–4077.

Arif Can Gungor (Student Member, IEEE) was born in Bolu, Turkey, in 1992. He received the bachelor's degree in electrical engineering and physics (second major) from the Middle East Technical University, Ankara, Turkey, in 2015 and the master's degree in electrical engineering from the University of California Santa Barbara, Santa Barbara, CA, USA, in 2017. Since 2018, he has been working toward the Ph.D. degree in electrical engineering with the Institute of Electromagnetic Fields, ETH Zürich, Zürich, Switzerland.

His doctoral research focuses on modeling of multiphysics scenarios, computational electromagnetics, and numeric methods.

Malgorzata Celuch (Member, IEEE) received the B.Sc., M.Sc. and Ph.D. (Hons.) degrees in electronic engineering from the Warsaw University of Technology, Warsaw, Poland, in 1996.

She is a QWED co-founder (1997), President (executive), and Senior Scientist, a lead coauthor of QuickWave commercial electromagnetic software package. Her research on FDTD EM and multiphysics modeling dates back to M.Sc. and Ph.D. research at the Warsaw University of Technology, where she was holding academic positions till 2017. She has authored or coauthored more than 170 scientific peer-reviewed papers and six monograph chapters (h-index 16 960 citations), recipient of more than 10 awards for excellence. Her current research focuses on applications of multiphysics computer modeling to the development of microwave techniques for materials processing and characterization.

Dr. Celuch was Expert for the European Commission FP7 and H2020 programs, and led research teams in eight European projects (on-going MMAMA and NanoBat). Within IEEE, she is a member of TC MTT-1, Associate Editor of the IEEE Journal on Multiscale and Multiphysics Computational Techniques, Vice-Chair of PS WiE AG, was a Co-Chair of AES/AP/MTT Joint Chapter PL, Reviewer for journals (including the IEEE Transactions on Microwave Theory and Techniques, AP, IM Trans.) and conferences (including IMS TPRC). She co-leads Model Development Focus Area of the European Materials Modeling Council.

Jasmin Smajic (Senior Member, IEEE) was born in Tuzla, Bosnia and Herzegovina, in 1971. He received the B.Sc. degree in electrical engineering from the Faculty of Electrical Engineering, Tuzla, Bosnia and Herzegovina, in 1996, and the M.Sc. and Ph.D. degrees from the Faculty of Electrical Engineering and Computing, Zagreb, Croatia, in 1998 and 2001, respectively, with the main topic of his M.Sc. and Ph.D. studies being numerical computing of static and time-varying electromagnetic fields in power transformers and electrical machines, as well as their design optimization.

From 2002 to 2004, he was a Postdoctoral Research Fellow with the Computational Optics Group, Laboratory for Electromagnetic Fields and Microwave Electronics, ETH Zürich, Zürich, Switzerland. The main topics of his postdoctoral studies were full-Maxwell electromagnetic simulations of photonic crystals and similar electromagnetic metamaterials. In 2004, he joined, as a Scientist, the ABB Corporate Research Centre, Baden-Dättwil, Switzerland, where he stayed until 2011. His work in ABB covered a wide range of projects in the field of computational and applied electromagnetics such as LI-modeling and simulation of transformer windings, fast electromagnetic transients in power and distribution transformers, coupled electromagnetic-mechanical, and electromagnetic-thermal analysis of transformers and circuit breakers, and very fast electromagnetic transients in gas insulated switchgears. From 2007 to 2020, he was an External Lecturer with Swiss Federal Institute of Technology, ETH, teaching at the master's and Ph.D. level several courses on computational electromagnetics and physical modeling. From 2011 to 2020, he was a Professor of electrical engineering with the University of Applied Sciences, Rapperswil, Switzerland, where he was leading Computational and Applied Electromagnetics Group. Since 2020, he has been a Lecturer and Senior Scientist with Swiss Federal Institute of Technology, ETH. He is currently with the Institute of Electromagnetic Fields, where he leads theoretical and simulation-related research activities. He has authored more than 100 scientific publications and dozens of patents.

Dr. Smajic is a member of CIGRE.

Marzena Olszewska-Placha (Member, IEEE) received the B.Sc., M.Sc., and Ph.D. degrees in the fields of waveguide filters, double reflector antennas, and graphene-based composite absorbing panels from the Warsaw University of Technology, Warsaw, Poland, in 2008, 2010, and 2014, respectively.

Since 2010, she has been a Research Engineer with QWED (Polish SME), Warsaw, Poland, involved in electromagnetic modeling and design of microwave devices and material characterization. She has participated in research projects concerned with modeling and applications of graphene composites and metamaterials at gigahertz and terahertz frequencies, application of microwave power to bituminous surfaces treatment, materials characterization, and commercial projects concerned with design of antennas and high-power microwave applicators. She has authored 11 journal articles and 22 conference presentations with 160 citations, three monograph chapters, and one patent.

Dr. Olszewska-Placha was a Reviewer for several IEEE journals, including the IEEE TRANSSCATION ON MICROWAVE THEORY AND TECHNIQUES and IEEE JOURNAL OF MULTISCALE AND MULTIPHYSICS COMPUTATIONAL TECHNIQUES.

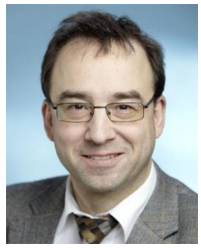

Juerg Leuthold (Fellow, IEEE) received the Ph.D. degree in physics from ETH Zürich, Zürich, Switzerland, in 1998, for work in the field of integrated optics and all-optical communications.

Since 2013, he has been the Head of the Institute of Electromagnetic Fields, ETH Zrich, Switzerland.From 2004 to 2013, he was with the Karlsruhe Institute of Technology, Germany, where he was the Head of the Institute of Photonics and Quantum Electronics and the Helmholtz Institute of Microtechnology. From 1999 to 2004, he was with Bell Labs, Lucent Technologies, Holmdel, NJ, USA, where he performed device and system research with III/V semiconductor and silicon optical bench materials for applications in high-speed telecommunications. His research interests include photonics, plasmonics, and microwave with an emphasis on applications in communications and sensing.

Dr. Leuthold is a Fellow of the Optical Society of America (OSA) and a member of the Heidelberg Academy of Science. He served the community as member of the Helmholtz Association Think Tank, as a member of the Board of Directors of OSA, and in many technical program committees or as the General Chair of meetings.